A Method for Measuring Ohmic Resistance of Solution Layers at Gas-Evolving Electrodes

W. Botter, Jr.

Instituto de Quimica, UNICAMP, 13081, Campinas, SP, Brazil

O. Teschke*

Instituto de Fisica, UNICAMP, 13081, Campinas, SP, Brazil

ABSTRACT

A method for measuring ohmic resistance of solution layers at gas-evolving electrodes was developed and tested. The method was applied to hydrogen and oxygen-evolving electrodes, and the resistance of their adjacent solution layers (for a 9 mm electrode separator gap) causes a negligible IR drop. For 3 mm gaps at a current density of 300 mA/cm^2, the IR drop of the solution layer increases to 25 mV. Contact resistances at the various electrode connections are shown to have a measurable contribution which increases with electrolysis time.

Electrolytic gas evolution represents a significant and complicated problem in many electrochemical processes. During alkaline water electrolysis, energy losses take place owing to the presence of gas bubbles in the electrolytic cell. The gas bubble contributions to an increase in potential include the following factors: (*i*) At the electrode surface the bubbles are closely packed in a thin layer forming a "bubble curtain." The crowded bubbles effectively screen the electrode, raise the effective current density, and thus offer a high ohmic resistance at the electrode surface. (*ii*) Bubbles disperse into the bulk electrolyte and hence increase its resistance.

The structure and behavior of the bubble curtain has been studied previously, particularly in connection with mass-transfer studies (1-3) of which Vogt (4) gives a summary. Landolt *et al.* (5) obtained an empirical bubble size distribution in turbulently flowing electrolyte and noted a wide range of bubble sizes. Hine *et al.* (6) suggested that a bubble curtain, though it may be thin, can affect the total cell voltage. Vogt (7) derived a model for the overall ohmic potential drop in a gas-evolving cell with vertical electrodes. DeJonge *et al.* (8) studied bubble effects in a cell with a disk electrode and analyzed bubble curtain behavior. Sides and Tobias (9) examined the effect of the bubble curtain and derived two models. More recently, Tenan and Teschke (10) investigated the influence of attached bubbles on the current distribution and the potential drop at gas-evolving electrodes. A more complete study was later presented by Dukovic and Tobias (11).

We applied a current interruption technique to measure experimentally the bubble effect on the ohmic resistance of a thin solution layer at gas-evolving electrodes. The resistance distribution was measured along a line normal to the electrode by displacing the reference electrode normally to the electrode surface and measuring the IR component of the electrode potential as a function of the distance to the electrode surface.

Electrode Resistive Layer IR Component Measuring Technique

Current interruption has long been established as a method of estimating the cell ohmic drop and electrode polarization potentials; an alternative but older method consists of measuring the electrode potential as a function of the distance (d) of the reference electrode to the working electrode and plotting this measured value as a function of d. Extrapolation of the V *vs.* d line for d equal to zero gives the electrode potential free of the IR component. However, if there is a resistive layer at the electrode surface, the potential thus measured includes the value of the ohmic drop due to the resistive layer (Fig. 1a and b). On the other hand, the current interruption technique measures the electrode potential without the two IR components, *i.e.*, bulk and surface, as shown in Fig. 1c.

In this paper we present what is the combination of those two methods and what is convenient to systematically determine the electrode surface resistance (Fig. 1d). Such a method consists of measuring the IR component by interruption of the current as a function of the distance of the reference electrode to the working electrode. If the electrode does not present a surface resistance, the extrapolation of the IR component *vs.* d line for d equal to zero will pass through the intersection of the IR-d axes (Fig. 1d); if for d equal to zero there is an IR component, it will correspond to the surface-resistance contribution.

Operational problems may introduce some difficulties in measuring the correct values, such as: (*i*) temperature gradients inside the cell, (*ii*) inhomogeneity of the current distribution, and (*iii*) shadow effect of the reference electrode. These problems have to be dealt with before an accurate measurement is obtained.

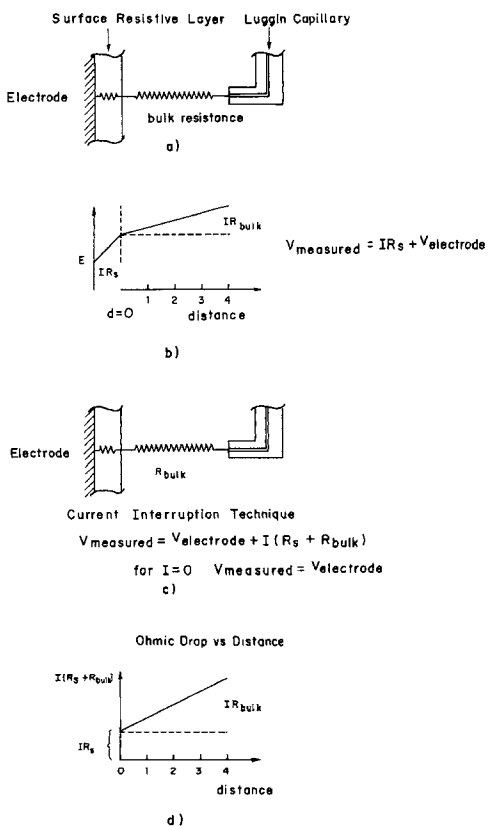

Fig. 1. Schematic representation of the resistance component distribution at an electrode surface. Figures (a), (b) (c), and (d) illustrate the method.

* Electrochemical Society Active Member.

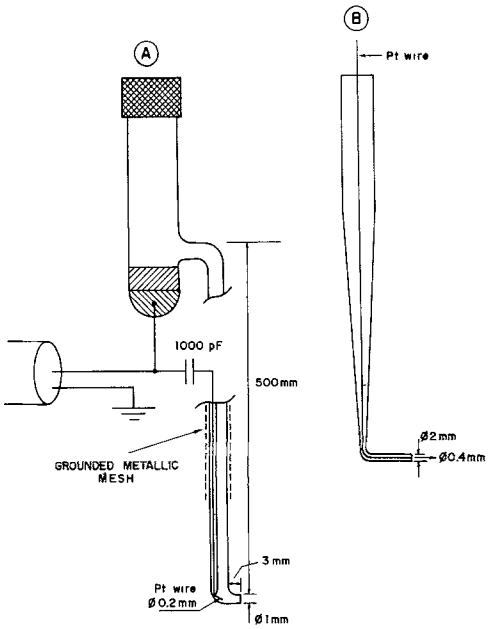

Fig. 2. Schematic diagram of the reference electrodes. The time response of both configurations is less than 1 μs. (a) Hg/HgO plus platinum wire. (b) Platinized platinum electrode.

Experimental

Recently various Hg/HgO reference electrode configurations were experimentally examined (12). Our results show that the Hg/HgO electrode may considerably limit the time response for IR-free potential measurements when high current densities (≈1 A/cm²) are used in alkaline solutions. A configuration with a response time of less than 1 μs was used in this work and is schematically shown in Fig. 2a. A Luggin probe made out of glass, as

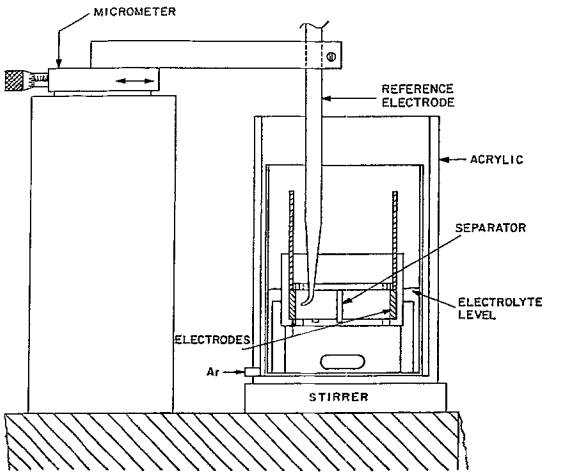

Fig. 3. Schematic diagram of the experimental setup.

shown in Fig. 2a, is connected to a reference electrode consisting of Hg/HgO 30% KOH. The tubing connecting the reference electrode and cell was surrounded by a grounded metallic mesh in order to decrease the electrical interference and to create a coaxial cable type of connection between the reference electrode and the working electrode. A platinum wire encapsulated by a glass rod, inside the tubing connecting the reference electrode to the cell, was used as a fast reference electrode. A ~1000 pF capacitor isolates the dc polarization variations of the Pt wire tip from the Hg/HgO electrode. Figure 2b shows the reference electrode configuration used for IR component measurements in 3 mm gap cells. The platinum reference electrode was welded in a glass tube having an outer diameter of 2 mm. The metallic tip was covered with black platinum by the usual method. The separator is a porous PTFE membrane previously described (13). A hole was drilled through the separator. The reference electrode support

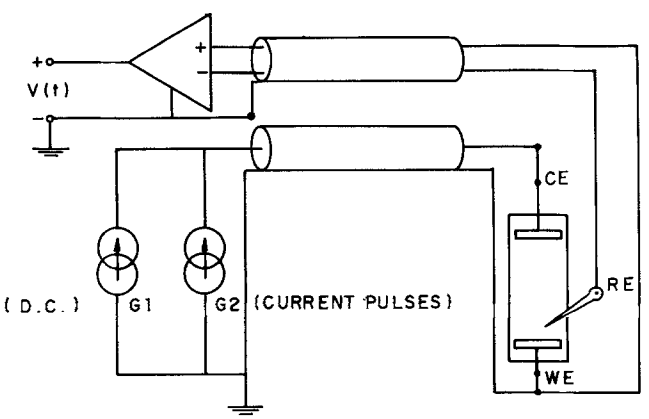

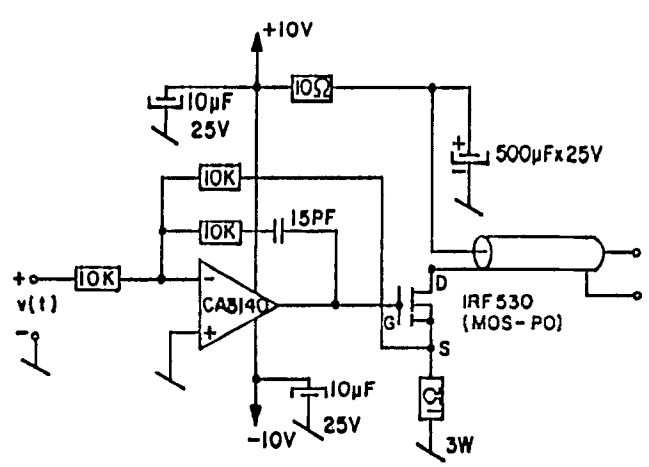

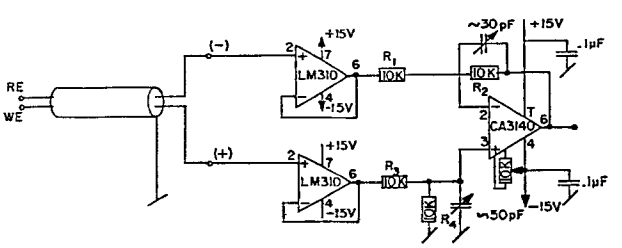

Fig. 4. (a, top left) Schematic diagram of the circuit. (b, top right) Pulsed current generator. (c, left) Differetnial amplifier.

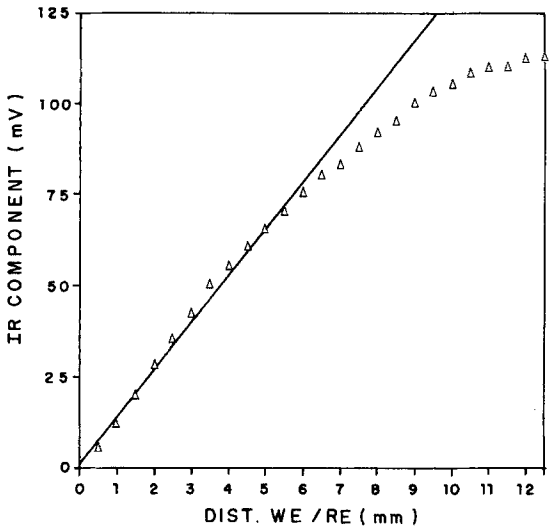

Fig. 5. IR component as a function of the distance to the working electrode for the cell, shown schematically in Fig. 6.

structure was placed outside the 3 mm gap. Its horizontal end was fitted inside the separator hole and the electrode was horizontally displaced using the structure shown in Fig. 3.

The test cell is an improvement over our earlier version (7) and is schematically shown in Fig. 3. The electrodes, each having an area of 3.3 cm^2, were rectangular nickel plates previously electroplated in a Watt's solution prepared with double-distilled water as follows: 310 g/l $NiSO_4$ (Merck), 50 g/l $NiCl_2$ (Merck), and 40 g/l boric acid (Quimbrás) all analytical grade. A 15 μm thick nickel layer was deposited on all electrodes in a solution at 60°C, pH = 3.5, and at a current density of 35 mA/cm^2. The cell module consists of two removable plug-in units as shown in Fig. 3 and 6. The cell frame and the plug-in units are made out of Teflon. The total electrode gap is 3.5 cm. The electrode plates are soldered to stainless steel wires. The electrolytic cell was operated at atmospheric pressure. The electrolyte flows by forced convection. It was thermostated at 45°C and the electrolyte solution prepared with doubly distilled water was 30% KOH (Merck analytical grade w/w). An external reservoir keeps the electrolyte concentration constant, avoiding decrease by electrochemical consumption or evaporation.

The apparatus for the IR component measurements is schematically shown in Fig. 4a, b, and c. The galvanostat schematic diagram (12), shown in Fig. 4a, generates current pulses with a risetime of less than 1 μs and with a maximum current amplitude of 2.5A. The circuit of the pulsed current generator is shown in Fig. 4b and the differential amplifier circuit in 4c. The time-dependent potential $V(t)$ is observed in an oscilloscope. A Hewlett Packard 54201A digitizing oscilloscope, a HP 7090A measurement

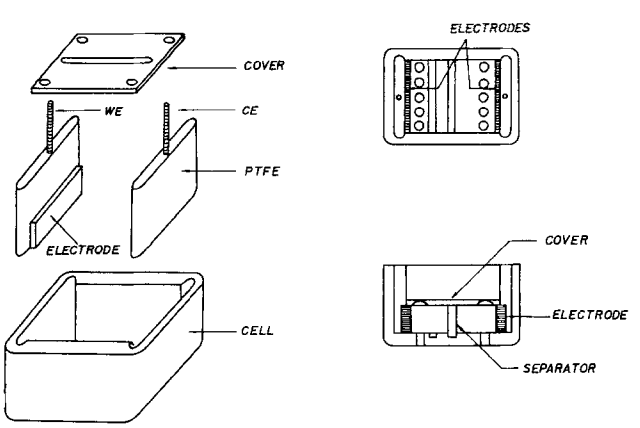

Fig. 6. Schematic diagram of the cell.

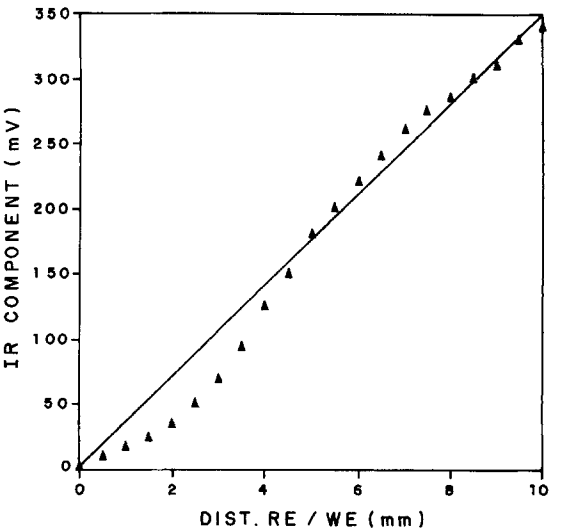

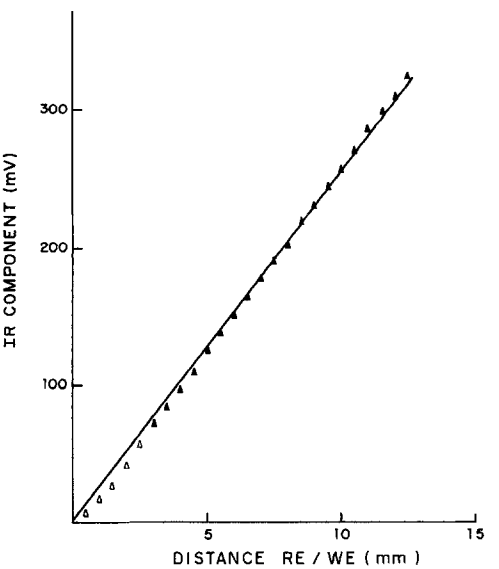

Fig. 7. (a, top) The IR component vs. distance curve for a 2.5 mm external diameter Luggin capillary. Points close to the electrode surface show the capillary shielding effect. (b, bottom) Shielding effect for a 1 mm external diameter Luggin capillary shown in Fig. 2a.

plotting system, and an Iwatsu SS-5710 oscilloscope were used for all time-dependent measurements. The current interrupt circuit used for dc measurements was previously described (14).

Cell optimization and preliminary results.—In our galvanostatic measurements a controlled current is forced between the working electrode (WE) and the counterelectrode (CE); the ohmic drop between the reference electrode (RE) and WE is obtained by interrupting the current and measuring the potential fast decay immediately thereafter.

A typical result for a cell with 1 cm^2 electrode area and a 3.3 cm^2 cell cross section is shown in Fig. 5. Since the electrode area is smaller than the cell cross section, the IR component *vs.* d curve profile is not a straight line but is bent at those points where the current density is lower. If the top of both electrodes is covered by a perforated plate, the cell cross section is reduced to 1 cm^2 and consequently, a uniform current distribution inside the cell is obtained. The cell shown in Fig. 6 is the result of removal of the stray factors like nonuniformity of the current distribution.

The temperature gradients along the axis normal to the electrode surface had to be minimized, since a significant variation in temperature causes a large variation of the electrolyte resistivity and consequently a variation in the linear relation Ri *vs.* distance measurements. The tempera-

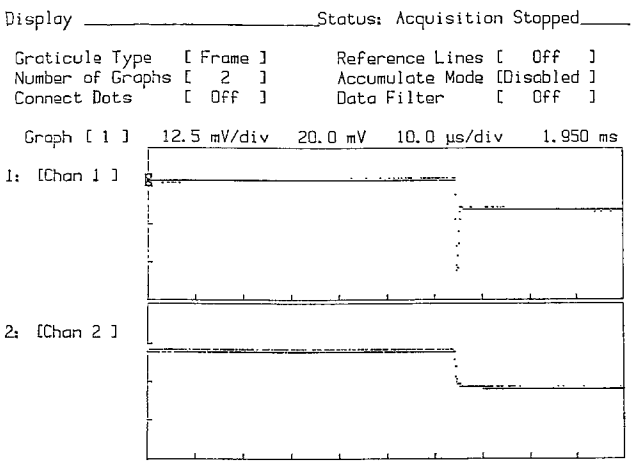

Fig. 8. Electrode potential and current *vs.* time curves at the current pulse trailing edge. The IR component is the difference between almost horizontal lines shown in Chan. 1. Chan. 2 shows the current pulse trailing edge. The measured current switching time is around 1 µs.

ture gradient, for a current density of 1 A/cm², between the region close to the electrode surface (*i.e.*, ≈ 1 mm away, where a thermometer was placed) and the central part of the cell, was less than 0.5°C in the cell shown in Fig. 6. This temperature homogeneity was obtained by the combined action of the holes drilled at the bottom of the cell close to the electrode surface and the stirrer action. The stirrer placed under the cell induces through the set of holes drilled at the cell bottom a convection that results in the measured temperature gradient.

The reference capillary placed a few capillary diameters from the working electrode generates distortions of the current distribution. For points close to the electrode surface, the shielding of the Luggin results in a locally lower current density of the electrode; consequently, a potential decrease results as shown in Fig. 7a for a 3.0 mm external diameter Luggin. For a Luggin capillary with a 2 mm external diameter tube, (Fig. 2b), the IR *vs.* *d* curve measured using the cell depicted in Fig. 6 is shown in Fig. 7b. This curve shows a linear relation between IR and *d*, except at points less than 2 mm away from the surface. The extrapolation of the IR line for a point close to the surface allows us a determination of the surface IR component with a 10 mV precision.

Results

Current was applied to the cell as follows: (*i*) Current pulses (≈300 mA/cm²) with a width of about 10 ms generate bubbles at the electrode surface, and (*ii*) a dc current (≈1 A/cm²) generates bubbles at the electrode surface and in the electrolyte.

The switching time at the end of the current pulse is shown in Fig. 8; a potential *vs.* time plot is shown in Chan. 1 and a current *vs.* time curve in Chan. 2. For a 1.95 ms long current pulse and I = 300 mA/cm² shown in Fig. 8, the measured current switching time is ~2 µs. The IR component is the difference between the almost two horizontal lines shown in Chan. 1.

For 1 ms long current pulses, triggered at every 100 ms and a current density of 300 mA/cm², the IR component for the cathode is shown in Fig. 9a and for the anode in Fig. 9b. The lower straight line in the figure was obtained for a freshly nickel-electrodeposited layer and the upper straight line, for the same electrode after 24 h inside the cell, *i.e.*, after 8 h of operation, the power supply was disconnected and the electrodes were left in the cell in 10 mm H_2O argon over-pressure; this was followed by another 8 h period of operation and finally, by the measurements.

Figure 10 shows a plot of IR component *vs.* distance from the capillary end to the working electrode surface for various current pulse amplitudes. The current pulse width is 2 ms and pulses are applied at every 100 ms.

In order to measure the bubble's effect in the bulk of the electrolyte and at the electrode surface, the IR component

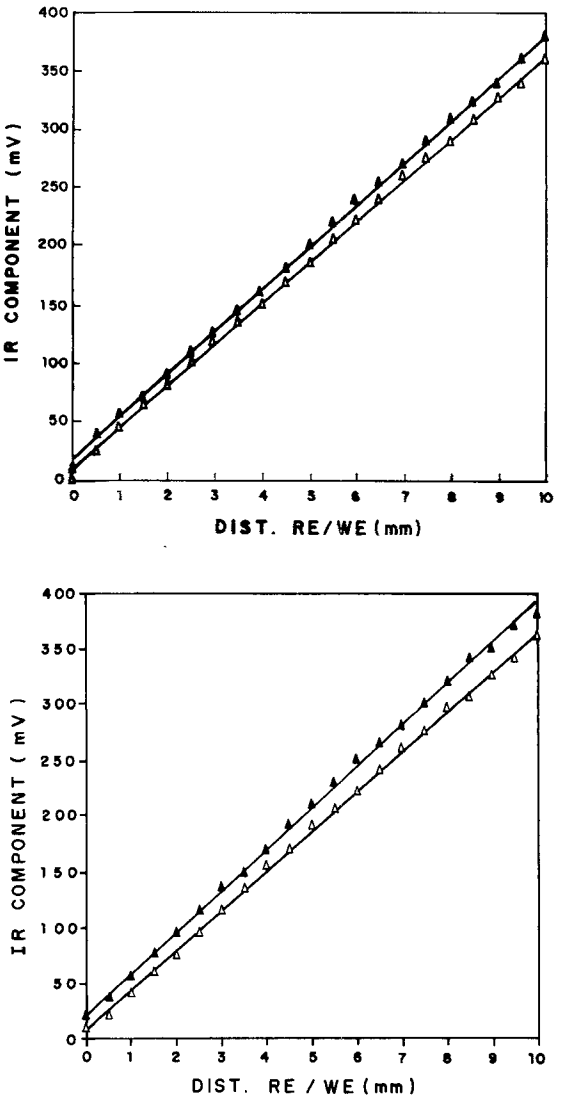

Fig. 9. (a, top) Cathodic IR component as a function of the distance to electrode surface for 300 mA/cm² and 1 ms current pulses at every 100 ms. (b, bottom) Anodic IR component.

was measured for various background dc currents, simulating the operation conditions of water electrolyzers. The results are shown in Table I for the cathode and Table II for the anode. The IR component was measured by applying 300 mA/cm² current pulses added to the dc background currents at the trailing current edge, as shown in Fig. 8.

Figure 11 displays the electrolyte IR component as a function of the distance of the capillary tip to the working electrode for two different electrode/membrane spacings (Fig. 6). For a 3 mm gap between the electrode and the membrane, the bubbles are closely packed in the electrolyte and offer a higher ohmic resistance than for a 9 mm gap. The bubble accumulation in a layer at the electrode surface results in a surface resistance. An IR surface component of ~25 mV was measured for a current density of 300 mA/cm² and I_{DC} of 500 mA/cm².

Finally, Fig. 12 shows the effect of electrolyte stirring. The IR component *vs.* distance was plotted for conditions (*i*) normal stirring, and (*ii*) violent stirring.

Discussion

Current interruption is a well-established method for estimating the cell ohmic drop and the electrode polarization potential; an older method for estimating the electrode polarization consists of measuring the electrode potential as a function of the distance of the reference electrode to the working electrode and plotting this value as a function of distance (*d*). The extrapolation of the *V vs d* line for *d* equal to zero gives the electrode potential free of the IR com-

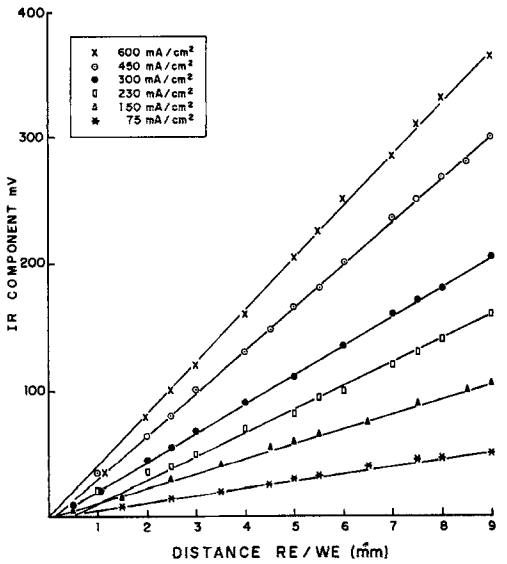

Fig. 10. IR component *vs.* distance from the capillary to the working electrode surface for various current pulse amplitudes. Pulse width 2 ms period 100 ms.

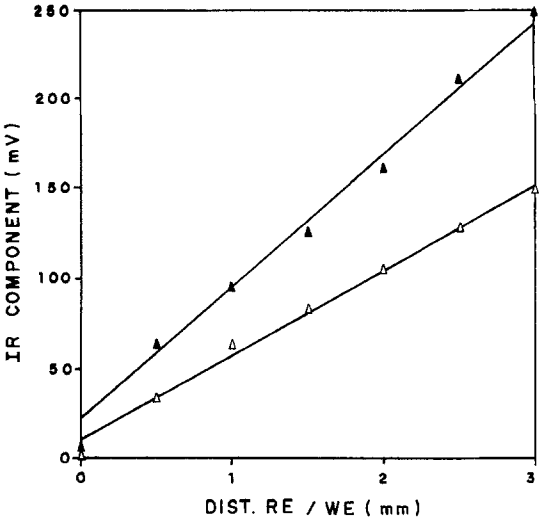

Fig. 11. IR component as a function of the distance for a 3 mm electrode/separator gap Δ and for a 9 mm gap Δ.

ponent. It may happen that at the electrode surface there is a surface resistance; in those cases the two methods will not give the same value for the measured potential, since the second method has included in the measured potential the surface resistance contribution, as shown schematically in Fig. 1. This might be the reason why, most of the time, the two methods present different results and the IR-free measurement method shows lower values than the other.

In this paper we present a method in which the surface resistance is determined by measuring the IR component as a function of the distance between WE and RE for gas-evolving electrodes. What we observe is that even though there was bubble formation over the surface, 300 mA/cm², 10 ms current pulses did not cause any increase in surface resistance. Various background dc currents were added to the 300 mA/cm² current pulses; the results do not show any contribution of the resistive layer at the electrode surface.

Only for an electrode separator gap of 3 mm it was possible to detect a contribution of the bubble effect, both in the electrolyte bulk and at the electrode surface, as shown in Fig. 11. This effect is due to bubble crowding and the consequent increase in the electrolyte void space.

An apparent bubble curtain effect was detected when the stirring electrolyte motion was substantially increased; due to the motion induced by stirring there was a decrease in bubble density for points away from the electrode. This results in a decrease of the bulk resistance but not a decrease in the resistance of the electrode's adjacent electrolyte layer, due to the presence of a stagnant liquid layer at the electrode surface, as shown in Fig. 12.

After a period of operation-interruption-operation (24 h), the electrode has a surface resistance which is probably associated with the growth of different substances on the nickel electrode, *i.e.*, a nickel hydride at the cathode and a nickel oxide at the anode. Electrode connection resistance presents a contribution to the IR component which increases with electrolysis time. For this reason, connections have to be tightened at each starting.

Fresh nickel electrodes which were not cathodized before the nickel electrodeposition present a resistive component which is probably associated with the presence of a nickel oxide layer beneath the nickel overlayer.

Table I. Cathodic IR component for various background dc currents measured by applying 300 mA/cm² current pulses.

WE × RE (mm)	DC Current (mA/cm²) 00	30	60	130	200	250
0.0	5	5	2	3	5	5
0.5	15	12	10	18	15	20
1.0	25	28	22	30	25	30
1.0	35	38	35	40	35	40
2.0	48	48	45	50	45	50
2.5	58	60	55	60	55	60
3.0	70	70	68	70	75	70
3.5	80	78	80	80	82	85
4.0	90	92	95	90	95	92

Table II. Anodic IR component for various background dc currents measured by applying 300 mA/cm² current pulses.

WE × RE (mm)	DC Current (mA/cm²) 00	30	60	130	200	250
0.0	5	4	6	5	6	6
0.5	12	12	13	14	15	13
1.0	20	23	23	24	25	22
1.5	28	33	34	35	35	35
2.0	38	45	45	45	46	45
2.5	48	54	55	55	56	54
3.0	58	63	68	67	68	63
3.5	68	73	78	78	78	78
4.0	75	83	80	88	85	88

Conclusions

1. A method for measuring electrode surface resistance was developed and tested. It consists of measuring the IR drop as a function of the distance of the reference electrode to the working electrode.

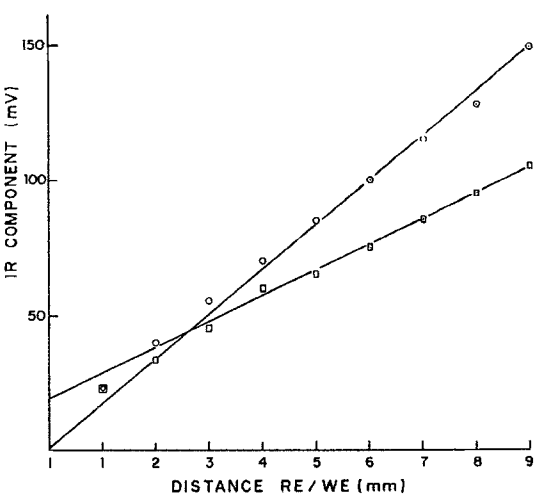

Fig. 12. Effect of the electrolyte stirring. (*i*) Normal, (*ii*) violent.

2. For electrodes with a resistive layer at the surface, the current interruption technique and the conventional method of determining the electrode potential (obtained by displacing the electrode along the interelectrode space) gives different results. The IR-free potential values determined by the current interruption technique are usually smaller than the ones obtained by the other method.
3. Curtain effect is only measurable (±10 mV) for bubbles confined to a restricted volume (for 300 mA/cm^2 current density and electrode-membrane spacing ≈3 mm, V = 1 cm^9).
4. Electrodes separated by a gap of ~7 mm or larger do not show any IR component contribution due to bubble curtain effect (for a current density of ~1 A/cm^2).
5. After a period of operation-interruption-operation, nickel-coated surfaces developed a resistive layer.

Acknowledgment

The authors wish to acknowledge the financial support of FAPESP and CNPq.

Manuscript submitted Dec. 27, 1989; revised manuscript received Oct. 29, 1990.

Fundacão de Amparo à Pesquisa do Estado do Estado de São Paulo assisted in meeting the publication costs of this article.

REFERENCES

1. L. J. J. Janssen and S. J. D. Van Stralen, *Electrochim. Acta*, **26,** 1011 (1981).
2. L. J. J. Janssen and E. Barendvechit, *ibid.*, **24,** 693 (1979).
3. L. J. J. Janssen, *libid.*, **23,** 81 (1978).
4. H. Vogt, in "A Comprehensive Treatise on Electrochemistry," Vol. 6, E. Yeager, J. O'M. Bockris, B. Conway, and S. Surangapani, Editors, Plenum Press, New York (1981).
5. D. Landolt, R. Acosta, R. H. Muller, and C. W. Tobias, *This Journal,* **117,** 839 (1970).
6. F. Hine and K. Murakami, *ibid.*, **127,** 292 (1980).
7. H. Vogt, *Electrochim. Acta*, **26,** 1311 (1981).
8. R. M. DeJonge, E. Barendrecht, L. J. J. Janssen, and S. J. D. Van Stralen, *Adv. Hydrogen Energy*, **2(1),** 195 (1981).
9. P. J. Sides and C. W. Tobias, *This Journal,* **127,** 288 (1980).
10. M. A. Tenan and O. Teschke, *Hydrogen Energy Progress V*, 593 (1984).
11. J. Dukovic and C. W. Tobias, *This Journal,* **134,** 331 (1987).
12. W. Botter, Jr., D. M. Soares, and O. Teschke, *J. Electroanal. Chem.*, **267,** 279 (1989).
13. O. Teschke, A. C. Costa, and F. Galembeck, *Electrochim. Acta*, **28,** 263 (1983).
14. O. Teschke, D. M. Soares, and C. A. P. Evora, *J. Appl. Electrochem.*, **13,** 371 (1983).

The Partial Oxidations of Cyclohexane and Benzene on the $FeCl_3$-Embedded Cathode during the O_2-H_2 Fuel Cell Reactions

Ichiro Yamanaka and Kiyoshi Otsuka

Department of Chemical Engineering, Tokyo Institute of Technology, Ookayama, Meguro-ku, Tokyo 152, Japan

ABSTRACT

Activation and partial oxidations of cyclohexane and benzene occur at ambient temperatures on cathodes containing various metal chlorides during O_2-H_2 fuel cell reactions. Among the metal chlorides embedded in graphite cathodes, $FeCl_3$ was the most effective for enhancing the partial oxidation of cyclohexane into cyclohexanol and cyclohexanone. This cathode was also effective for the hydroxylation of benzene to phenol. The effects of various kinetic factors on the rate of oxidations of cyclohexane and benzene have been examined. The kinetic results have been explained in terms of the reaction mechanism proposed. It is suggested that the activation and partial oxidation of cyclohexane and aromatics are initiated by an active oxygen, O*, generated on the iron cations at the cathode due to the reduction of dioxygen during the O_2-H_2 fuel cell reactions. Experiments using H_2O_2 as the oxidant have indicated that the H_2O_2 cannot be a precursor of the active oxygen O*. The product distribution observed in the oxidation of toluene implies that the O* has a character more electrophilic than OH radicals.

The direct partial oxidation of alkanes through dioxygen activation under mild conditions is one of the most interesting but still undeveloped fields of catalysis (1). Many systems based on the principles of coupled oxidations using a transition metal complex have been developed as mimics of enzymes such as cytochrome P-450 (2), methane monoxygenase (3), or copper monoxygenase (4).

Cytochrome P-450 catalyzes a wide variety of oxygenations such as hydroxylations of aromatics or of saturated hydrocarbons, and epoxidations of olefins (2). The active site of P-450 has long been known to contain a single iron protoporphyrin IX prosthetic group. Dioxygen is adsorbed, reduced, and activated on this site. It is generally accepted that the catalytic sequence of cytochrome P-450 involves the following steps (2): (*i*) binding of a substrate to give a high-spin ferric complex, (*ii*) one-electron reduction of the iron to the iron(II) state by an electron donor such as NADPH with the aide of the electron-transfer system in cytochrome P-450, (*iii*) binding of molecular oxygen to give the oxo-form complex $Fe^{3+}O_2^-$, (*iv*) transfer of a second electron to the complex to generate the iron peroxo species $Fe^{3+}O_2^{2-}$, (*v*) cleavage of the O—O bond with concomitant generation of the reactive oxidant $[FeO]^{3+}$ and a water molecule, (*vi*) a two-electron oxidation of the substrate to produce its oxygenate and regenerates the ferric resting state of the enzyme. Here the activation of dioxygen as a whole could be expressed as

$$O_2 + Fe^{3+}\text{ (P-450)} + 2H^+ + 2e^- \rightarrow [FeO]^{3+}\text{ (P-450)} + H_2O \quad [1]$$

Our recent work (5) has shown that the hydroxylation of benzene and cyclohexane can be achieved at the cathode during the fuel cell reactions of O_2 and H_2 using Pd-black cathode at room temperature. The reaction system employed for this work is shown in Fig. 1. As will be described later, preliminary experiments showed that the various metal chlorides impregnated in graphite enhanced the partial oxidation of cyclohexane at the cathode for the reaction system shown in Fig. 1. Among the metal chloride-impregnated electrodes tested, the $FeCl_3$-impregnated graphite (denoted as $FeCl_3$/Gr hereafter) showed the highest catalytic activity in the partial oxidation of cyclohexane. The oxidation of cyclohexane at the cathode may be initiated by an active oxygen (O*) generated during the O_2-H_2 fuel cell reaction. In this report, we demonstrate